 doi:10.20944/preprints202101.0271.v1

Article

Strain rate sensitivity of the additive manufacturing material Scalmalloy®

Puneeth Jakkula [1], Georg Ganzenmüller [1,2,*], Florian Gutmann [1,2], Aron Pfaff[2], Jörg Mermagen [2], Stefan Hiermaier[1,2]

[1] Albert-Ludwigs-Universität Freiburg, Sustainable Systems Engineering, INATECH, Emmy-Noether Str. 2, 79110 Freiburg, Germany
[2] Fraunhofer Institute for High-Speed Dynamics, Ernst-Mach-Institut, EMI, Ernst-Zermelo Str. 4, 79104 Freiburg, Germany
* Correspondence: georg.ganzenmueller@inatech.uni-freiburg.de

Abstract: This work investigates the influence of strain rate on the stress/strain behaviour of Scalmalloy. This material is an aluminium-scandium-magnesium alloy, specifically developed for additive manufacturing. The bulk yield stress of the material processed by Selective Laser Melting is approximately 340 MPa which can be increased by heat-treating to approximately 530 MPa. These numbers, combined with the low mass density of 2.7 g/cm^3, make Scalmalloy an interesting candidate for lightweight crash-absorbing structures. As this application is inherently dynamic, it is of interest to study the loading rate sensitivity, which is difficult to predict: Al-Sc alloys exhibit classic strain rate sensitivity with an increased yield stress at elevated strain rates. However, Al-Mg alloys are known to show the contrary effect, they exhibit less strength as strain rate is increased. To answer the question how these effects combine, we study the dynamic behaviour at four different strain rates ranging from 10^{-3} /s to 1000 /s using servo-hydraulic and Split-Hopkinson testing methods. The resulting data is analysed in terms of strain rate sensitivity of tensile strength and failure strain. A constitutive model based on a simplified Johnson-Cook approach is employed to simulate the tensile tests and provides good agreement with the experimental observations.

Keywords: Aluminium Alloy; Dynamic Testing; Additive Manufacturing, Split-Hopkinson Methods

1. Introduction

Additive manufacturing (AM) of metal structures allows for producing complex parts with tailored properties. These parts inherit their mechanical behaviour not only from the base material, but also from structural design choices, on a meso-scale between the metal microstructure length scale and the overall dimensions of the parts [1–3]. This allows for the design of light-weight, high-strength structures, and these are increasingly used for safety-relevant applications in aerospace and automotive engineering [4–8]. In these applications, dynamic loading due to crash and impact are routinely encountered. It is therefore a necessary requirement to know the strain-rate dependency of the base material to quantify crashworthiness.

This work considers the Scandium modified Aluminium-Magnesium alloy AA5028, which is commercialized by APworks and sold under the trade name Scalmalloy [9]. Its composition is based on the 5xxx series AlMg alloys. The addition of Scandium increases strength and improves weldability [10]. The bulk yield stress of the as-built material is approximately 350 MPa which can be increased by heat-treating to approximately 550 MPa. These numbers, combined with the low mass density of 2.8 g/cm^3, make AA5028/Scalmalloy an interesting candidate for lightweight crash-absorbing structures. Its strain-rate sensitivity, however, is difficult to predict:

Al-Sc alloys exhibit classic strain rate sensitivity with an increased yield stress at elevated strain rates [11]. In contrast, Al-Mg alloys are known to show the contrary effect, they exhibit negative strain rate sensitivity, at least up to moderate strain rates of 10^3 /s [12]. To answer the question how these

Preprints (www.preprints.org) | NOT PEER-REVIEWED | Posted: 14 January 2021 doi:10.20944/preprints202101.0271.v1

effects combine in AA5028, we study its dynamic behaviour at four different strain rates ranging from 10^{-3} /s to 1000 /s using servo-hydraulic and Split-Hopkinson testing methods. Both as-is and heat-treated specimens are investigated, and the resulting data is analysed in terms of the strain-rate dependency of Ultimate Tensile Strength (UTS) and strain at failure. Finally, a simplified Johnson-Cook material model is parametrized to reproduce the experimental findings, allowing for the simulation of dynamic loading events.

2. Materials and methods

2.1. Specimens

A total of 60 raw stock cylinders with dimensions of $\varnothing 20 \times 120$ mm^2 were produced in one batch by a commercial LBM system (EOS M 400), equipped with a 1kW laser unit (YLR-series, CW-laser, wavelength 1070 nm). The specimen were printed in a 90 degree orientation to the build plate. All objects were manufactured with 60 μm layers with a heated building platform (40C). Half of the batch was subjected to a heat treatment of 325C for 4 hours. The final specimen geometry according to Fig. 1 were then obtained by CNC machining.

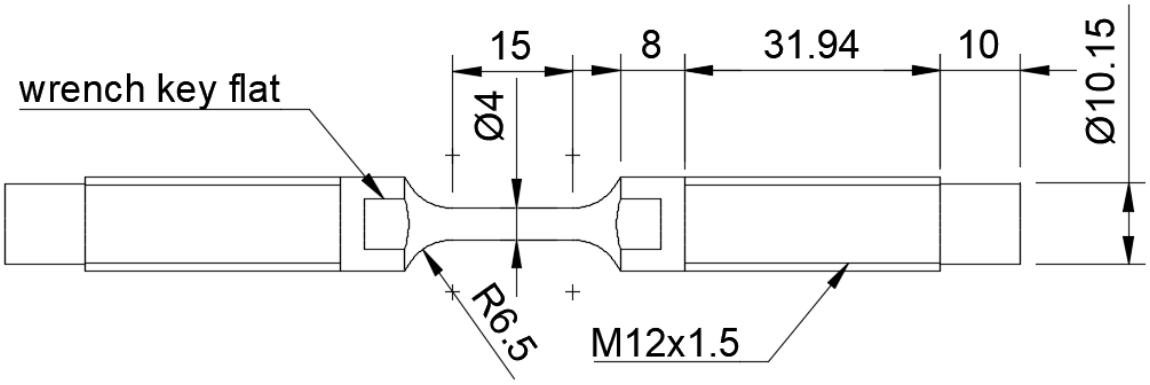

Figure 1. Specimen geometry with cylindrical gauge region $\varnothing 4 \times 15$. All dimensions are in mm.

2.2. Quasi-static and low strain rate testing

Tensile testing for the strain rates 0.001 /s, 0.1 /s, and 10 /s were performed using a servo-hydraulic testing machine (Instron 8801), equipped with a 50 kN load cell (Dynacell). Testing was performed in displacement controlled mode with constant cross-head velocities. Nominal specimen strain was evaluated as the elongation of the parallel gage region using Digital Image Correlation (DIC, GOM Correlate).

2.3. Dynamic strain rate testing

The Split-Hopkinson Tension Bar (SHTB) used here is sketched in Fig. 2 and described in detail in [13]. Compared to other SHTBs, this setup is optimized for low velocities, low forces and a long pulse duration of 1.2 ms. Force is measured via a pair of conventional strain gages mounted on the output bar, connected diagonally in a Wheatstone bridge circuit to eliminate bending information. The Wheatstone bridge circuit is driven in constant voltage mode and its output is increased by a factor of 100 using an amplifier with 1 MHz bandwidth. This signal is recorded by a data acquisition (DAQ) card operating at 10 MHz and 16 bit resolution. The conversion factor from strain to force is established via a calibration procedure, wherein a dedicated force sensor is placed between input and output bars, while a static load is applied onto the bars. The signal of the force sensor is recorded using the same amplifier and data acquisition card as during a real experiment. The force sensor, in turn is calibrated against the already calibrated load cell in the universal testing machine described above. Thus, the

Preprints (www.preprints.org) | NOT PEER-REVIEWED | Posted: 14 January 2021 doi:10.20944/preprints202101.0271.v1

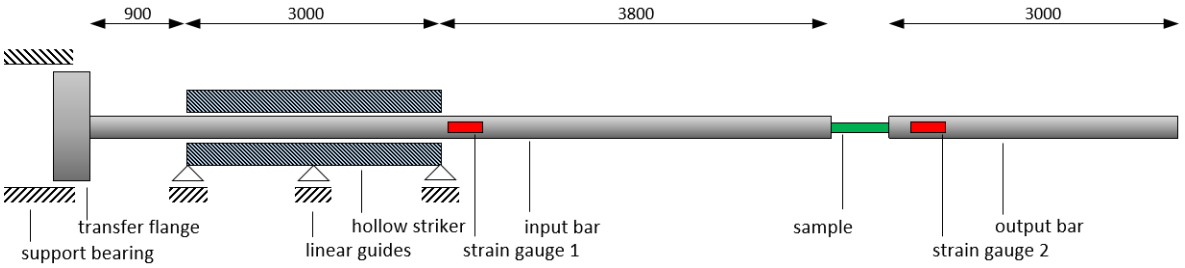

Figure 2. Sketch of the SHTB setup employed in this work. All dimensions in mm. Input and output bars are 16 mm diameter aluminium rods. The striker is a hollow aluminium tube of 40 mm outer diameter and 20 mm inner diameter. Two strain gage stations on the input bar and output bar measure the incident wave, ε_{inc}, and transmitted wave, ε_{tra}.

entire force measuring system consisting of strain gages, amplifier and DAQ card is calibrated, which compensates for any eventual misalignment of the strain gages or similar constant systematic errors. High-Speed video imaging of the sample is employed (Photron SAZ, 640x280 pixels, frame rate 100 kHz) for subsequent optical strain analysis by DIC. Shortly before performing the experiment, a speckle pattern with white and black spray paint was applied to the specimen gauge section in order to provide the necessary contrast for the DIC analysis. The specimens were then directly threaded into the bar ends and torqued to 10 Nm. The experiment was then conducted by firing the striker against the input flange at a velocity suitable to reach a nominal strain rate of 1000 ± 100 /s in the sample gauge section.

2.4. Data reduction

Fig. 3 shows the nominal stress/strain curves obtained for all combinations of strain rate and specimen type: as-is (untreated) and heat-treated. Each testing series consists of $N = 5$ experiments. Within one series, the individual experiments exhibit very little scatter. The characteristic properties ultimate tensile strength, σ_{max} and strain at failure, ε_f are represented using straightforward averages and uncertainty estimates, e.g. for the strength: $\bar{\sigma}_{max} = \sum_{j=1}^{N} \sigma_{max,j}/N$ and $s\left(\bar{\sigma}_{max}\right) = \sqrt{\sum_{j=1}^{N} \left(\sigma_{max,j} - \bar{\sigma}_{max}\right)^2 / (N-1)}$.

3. Results

The nominal stress/strain graphs obtained by our experiments are shown in Fig. 3. Within one testing series, the individual curves are almost indistinguishable which we attribute to the quality and reproducibility of our SLM process. At quasi-static rates of strain, obvious serrations in the curves are visible. These are presumably due to the Portevin-Le-Chatelier (PLC) effect, which describes the locking of a moving dislocation due to solute Mg atoms [12]. At higher strain rates, this effect diminishes as the diffusion speed of solute Mg becomes slow compared to the dislocation speed. Averages for ultimate tensile strength (the maximum of the nominal stress/nominal strain -curve) and the failure strain are reported in Table 1. Our quasi-static data is in agreement with prior work on Scalmalloy [14], where an UTS of 334 MPa and 540 MPa was reported for as-is and heat-treated specimens, respectively.

Preprints (www.preprints.org) | NOT PEER-REVIEWED | Posted: 14 January 2021 doi:10.20944/preprints202101.0271.v1

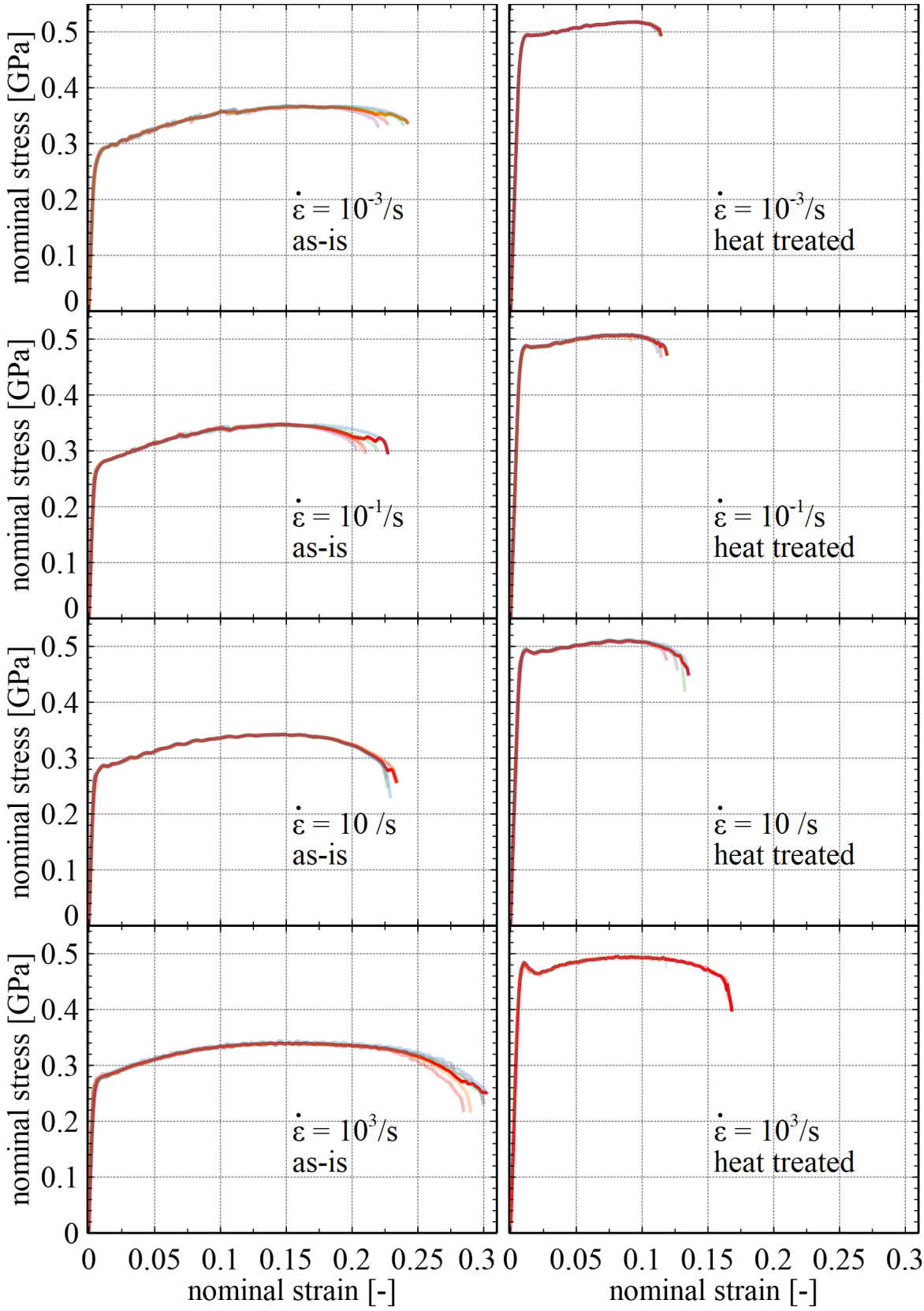

Figure 3. Scalmalloy nominal stress - nominal strain plots at different strain rates ranging from 10^{-3} to 10^{3} /s. Left and right columns are for as-is (non heat-treated) and heat-treated specimens, respectively. Note that each experiment set has 5 individual experiments which are shown with differently coloured lines.

Preprints (www.preprints.org) | NOT PEER-REVIEWED | Posted: 14 January 2021 doi:10.20944/preprints202101.0271.v1

Table 1. Results for ultimate tensile strength σ_{max} and failure strain ε_f at different strain rates considered in this work. Errors indicate on standard deviation.

	as is				heat-treated			
strain-rate	Max. strength / MPa		failure strain / %		Max. strength / MPa		failure strain / %	
0.001	368.4	±1.1	23.2	±1.1	518.6	±0.5	11.2	±0.2
0.1	348.5	±1.2	21.3	±1.1	508.1	±1.3	11.1	±0.5
10	342.6	±0.9	23.0	±0.4	511.0	±1.5	12.8	±0.6
1000	342.5	±1.6	29.5	±0.4	497.0	±3.0	15.0	±2.2

3.1. Strain-rate dependency

To quantify the strain rate sensitivity, the characteristic quantities given in Table 1 are analysed. The maximum stress is well represented by a relationship proportional to the negative logarithm of the strain rate:

$$\sigma_{max} = \sigma_0 + a \log(\dot{\varepsilon}) \tag{1}$$

The constant of proportionality is $a = -4.9 \pm 0.3$ MPa, and $a = -2.9 \pm 0.3$ MPa, for as-is and heat-treated Scalmalloy, respectively. Uncertainty estimates are obtained from the residual error of the Levenberg-Marquardt algorithm used for data fitting. The dependence of the strain at failure on strain rate does not follow this simple Johnson-Cook type behaviour. Instead, a Cowper-Symonds relationship appears to better fit the data:

$$\varepsilon_{fail} = \varepsilon_{fail,0} \left(1 + \alpha \left(\dot{\varepsilon} \times [\mathrm{s}]\right)^{\beta}\right) \tag{2}$$

For as-is specimens, we find $\varepsilon_{fail,0} = 0.223 \pm 0.005$, $\alpha = 0.009 \pm 0.007$, and $\beta = 0.51 \pm 0.10$. For heat-treated Scalmalloy, we find $\varepsilon_{fail,0} = 0.109 \pm 0.004$, $\alpha = 0.009 \pm 0.007$, and $\beta = 0.23 \pm 0.13$. We conclude this section by noting that Scalmalloy exhibits a weak negative strain rate sensitivity for the UTS. The failure strain, however, increases with along with the strain rate.

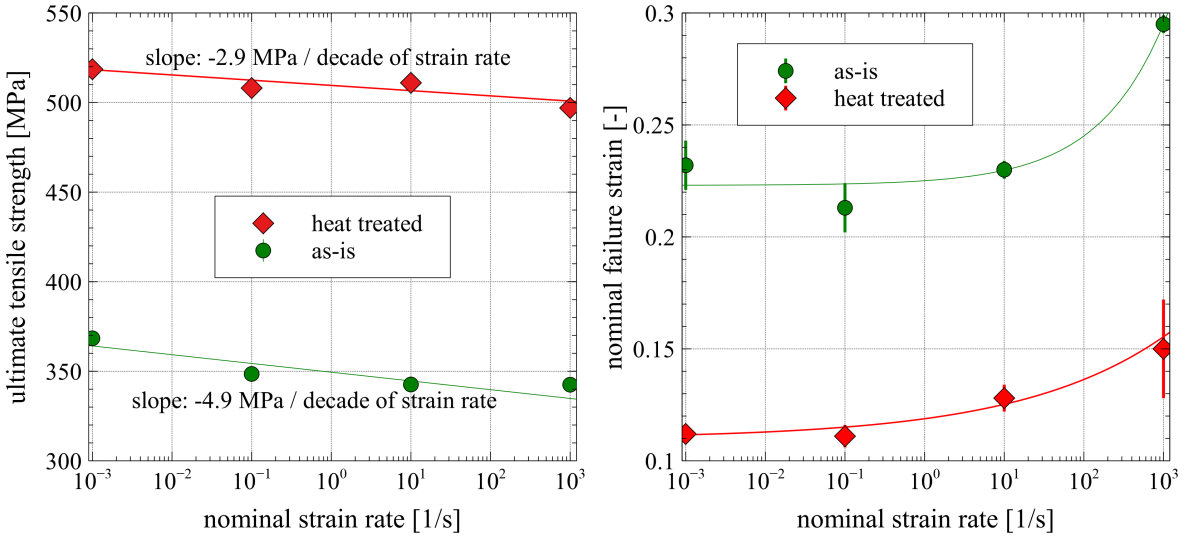

Figure 4. Analysis of the strain rate dependency of ultimate strength and failure strain. The ultimate strength is proportional to the logarithm of the strain rate, while the failure strain is better described using a Cowper-Symonds relationship, see text.

4. Simulation model

The data presented in Sec. 3 is employed to parametrize a simplified Johnson-Cook (JC) plasticity model in combination with an explicit Finite Element scheme LS-Dyna (v.11.0, Livermore Software Technology, USA). This JC model only accounts for isotropic hardening but no temperature effects. The

Preprints (www.preprints.org) | NOT PEER-REVIEWED | Posted: 14 January 2021 doi:10.20944/preprints202101.0271.v1

strain-rate dependency of the yield-stress is disregarded as it is weak, but more importantly, negative. Softening with increasing strain-rate would lead to strong instabilities in explicit time integration schemes as it promotes localization and necking. Failure is addressed by deleting elements which exceed a given value of effective plastic strain. The failure model is strain-rate sensitive according to the above determined Cowper-Symonds relations, c.f. Eq. 2.

4.1. Constitutive model

The constitutive model is based on isotropic linear elasticity with Young's modulus $E = 70$ GPa and Poisson's ratio $\nu = 0.3$. These values are typical of Aluminium alloys and in agreement with experimental data on Scalmalloy[14]. We utilize a J_2 plasticity model with radial return, based on the yield stress σ_y according to the simplified JC model:

$$\sigma_y = (A + B\,\bar{\varepsilon}^n) \tag{3}$$

Here, $\bar{\varepsilon}$ is the accumulated effective plastic strain. Failure is accounted for by deleting those elements which exceed the strain-rate dependent maximum effective plastic strain,

$$\bar{\varepsilon}_{fail} = \bar{\varepsilon}_0 \left(1 + \alpha\,(\dot{\varepsilon} \times [\mathrm{s}])^{\beta}\right) \tag{4}$$

The Cowper-Symonds parameters α and β are taken from Sec. 3. The remaining parameters A, B, n, and the initial failure strain $\bar{\varepsilon}_0$ are determined using an inverse approach, which is described in the following. Note that $\bar{\varepsilon}_0$ is not the same as the experimentally determined nominal failure strain ε_{fail}: The former refers to a local quantity under the influence of necking, while the latter describes the average strain of the entire parallel gauge region at failure.

4.2. Parametrization of the constitutive model

The reference effective plastic failure strain $\bar{\varepsilon}_0$, corresponding to a strain rate of 10^{-3} /s as well as the JC parameters A, B, and n are found by an inverse approach: we use the optimization package LS-Opt (v.6.0.0, Livermore Software Technology, USA) in combination with LS-Dyna to simulate tensile testing of the specimen described in Fig. 1. Discretization is performed in a 2d axis-symmetric coordinate system with quadrilateral elements of typical size 0.1 mm, which has been established through a convergence study. The simulation output, engineering stress and engineering strain (average of the parallel gauge section) are optimized to agree with the experimental data obtained at strain rate 10^{-3} /s. The resulting parameters are summarized in Table 2. The simulated tensile curves are compared to experiments in Fig. 5. The agreement at $\dot{\varepsilon} = 10^{-3}$ /s is good, which shows that the JC model is an apt choice for this material. While the simulation prediction at $\dot{\varepsilon} = 10^{3}$ /s is satisfactory, it overestimates the strength by ≈5 % in both cases, due to the neglect of the weak negative strain rate sensitivity.

Table 2. Parameters of the Johnson-Cook plasticity and failure model for heat-treated and as-is Scalmalloy.

type	A [MPa]	B [MPa]	n	$\bar{\varepsilon}_0$	α	β
as-is	198	400	0.332	0.41	0.009	0.51
heat-treated	399	362	0.345	0.13	0.009	0.13

Preprints (www.preprints.org) | NOT PEER-REVIEWED | Posted: 14 January 2021 doi:10.20944/preprints202101.0271.v1

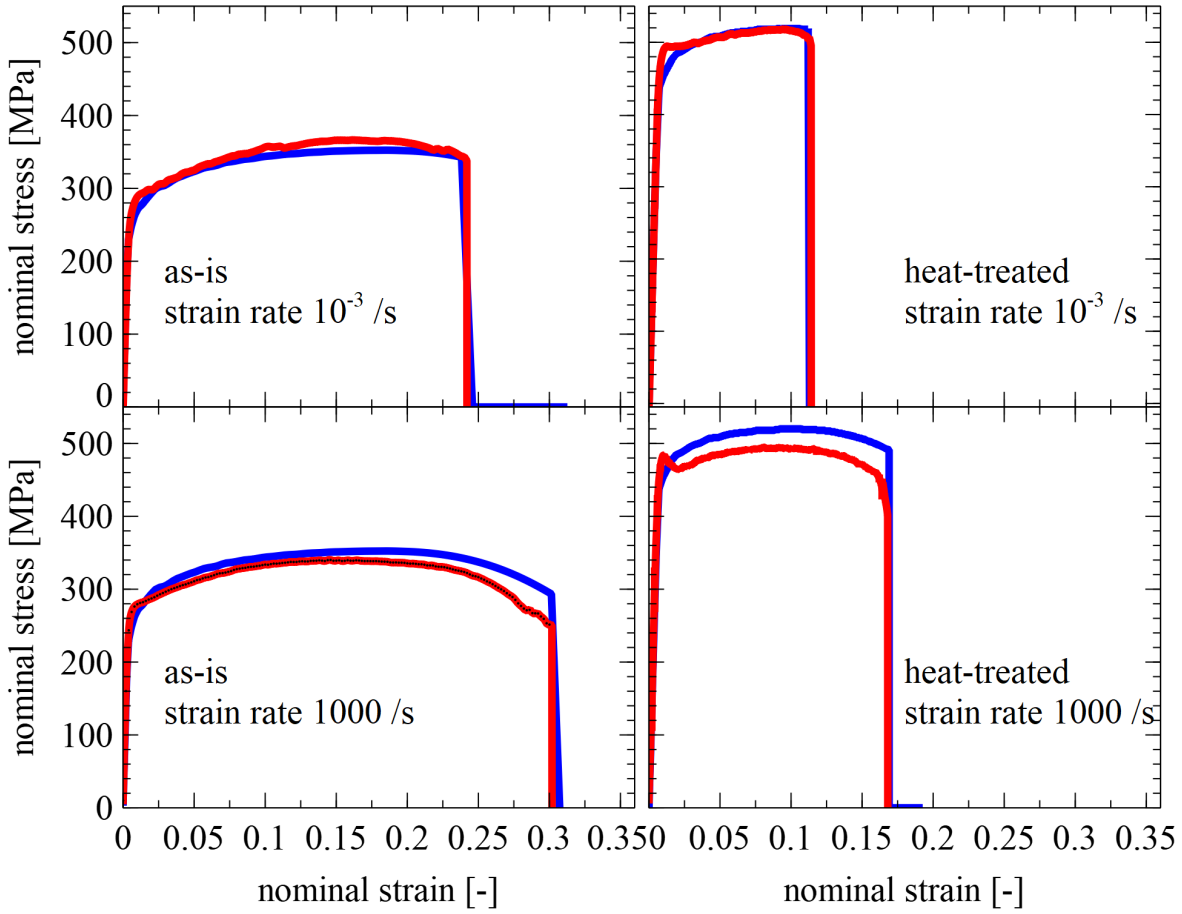

Figure 5. Comparison between simulation results with the Johnson-Cook model (blue curves) and the experimental data (red curves). The left column is for as-is Scalmalloy, the right column is for the heat-treated material.

5. Discussion and conclusion

This work investigated the strain rate sensitivity of the Sc-Al-Mg alloy Scalmalloy, which is specifically used for additive manufacturing purposes. Here, bulk tensile specimens obtained via Selective Laser Melting and machined to final dimensions were used. Using a combination of servo-hydraulic and Split-Hopkinson methods, tensile tests ranging from 10^{-3} /s to 10^{3} /s were performed. It was found that the Ultimate Tensile Strength decreases weakly (≈ -5 MPa / decade of strain rate) with increasing strain rate. Contrary, the failure strain was observed to increase along with rising strain rate. A constitutive model based on the Johnson-Cook plasticity model and a simple strain-rate dependent failure criterion was parametrized and shown to agree well with the experimental data.

This work addresses two important questions. From a practical point of view, this light-weight, yet high strength, aluminium alloy lends itself for safety-relevant applications which include crash and impact scenarios. Our work provides the necessary data and a model to design and simulate such structures, including the effects of strain rate. On the other hand, from a more scientific point of view, it is interesting to see how different strain rate effects of Sc and Mg combine in one aluminium alloy: for moderate strain rates $\approx 10^{-3}$, the addition of Mg mainly leads to a negative strain-rate sensitivity [12], while the addition of Sc incurs a pronounced positive strain rate sensitivity [15] for the UTS. For Scalmalloy, with alloying values of 4.4% Mg and 0.73% Sc by weight [14], these effects appear to mutually cancel out.

6. Acknowledgements

We acknowledge funding from Carl-Zeiss Foundation, grant title *Skalenübergreifende Charakterisierung robuster funktionaler Materialsysteme*.

1. Chekurov, S.; Metsä-Kortelainen, S.; Salmi, M.; Roda, I.; Jussila, A. The perceived value of additively manufactured digital spare parts in industry: An empirical investigation. *International Journal of Production Economics* **2018**, *205*, 87–97. doi:10.1016/j.ijpe.2018.09.008.
2. Mitchell, A.; Lafont, U.; Hołyńska, M.; Semprimoschnig, C. Additive manufacturing — A review of 4D printing and future applications. *Additive Manufacturing* **2018**, *24*, 606–626. doi:10.1016/j.addma.2018.10.038.
3. Rashed, M.G.; Ashraf, M.; Mines, R.A.W.; Hazell, P.J. Metallic microlattice materials: A current state of the art on manufacturing, mechanical properties and applications. *Materials & Design* **2016**, *95*, 518–533. doi:10.1016/j.matdes.2016.01.146.
4. Ozdemir, Z.; Hernandez-Nava, E.; Tyas, A.; Warren, J.A.; Fay, S.D.; Goodall, R.; Todd, I.; Askes, H. Energy absorption in lattice structures in dynamics: Experiments. *International Journal of Impact Engineering* **2016**, *89*, 49–61. doi:10.1016/j.ijimpeng.2015.10.007.
5. Tsouknidas, A.; Pantazopoulos, M.; Katsoulis, I.; Fasnakis, D.; Maropoulos, S.; Michailidis, N. Impact absorption capacity of 3D-printed components fabricated by fused deposition modelling. *Materials & Design* **2016**, *102*, 41–44. doi:10.1016/j.matdes.2016.03.154.
6. Li, S.; Zhao, S.; Hou, W.; Teng, C.; Hao, Y.; Li, Y.; Yang, R.; Misra, R.D.K. Functionally Graded Ti-6Al-4V Meshes with High Strength and Energy Absorption. *Advanced Engineering Materials* **2016**, *18*, 34–38. _eprint: https://onlinelibrary.wiley.com/doi/pdf/10.1002/adem.201500086, doi:10.1002/adem.201500086.
7. Tancogne-Dejean, T.; Spierings, A.B.; Mohr, D. Additively-manufactured metallic micro-lattice materials for high specific energy absorption under static and dynamic loading. *Acta Materialia* **2016**, *116*, 14–28. doi:10.1016/j.actamat.2016.05.054.
8. Brennan-Craddock, J.; Brackett, D.; Wildman, R.; Hague, R. The design of impact absorbing structures for additive manufacture. *J. Phys.: Conf. Ser.* **2012**, *382*, 012042. Publisher: IOP Publishing, doi:10.1088/1742-6596/382/1/012042.
9. Vorel, M.; Hinsch, S.; Konopka, M.; Scheerer, M. AlMgSc alloy 5028 status of maturation **2017**. p. 9 pages. Artwork Size: 9 pages Medium: PDF Publisher: Proceedings of the 7th European Conference for Aeronautics and Space Sciences. Milano, Italy, 3-6 july 2017, doi:10.13009/EUCASS2017-633.
10. Royset, J. Scandium In Aluminium Alloys: Physical Metallurgy, Properties And Applications. *Metallurgical Science and Tecnology* **2007**, *25*. Number: 2.
11. Lee, W.S.; Chen, T.H. Dynamic Mechanical Response and Microstructural Evolution of High Strength Aluminum–Scandium (Al–Sc) Alloy. *Mater. Trans.* **2006**, *47*, 355–363. doi:10.2320/matertrans.47.355.
12. Yamada, H.; Kami, T.; Mori, R.; Kudo, T.; Okada, M. Strain Rate Dependence of Material Strength in AA5xxx Series Aluminum Alloys and Evaluation of Their Constitutive Equation. *Metals* **2018**, *8*, 576. doi:10.3390/met8080576.
13. Ganzenmüller, G.C.; Blaum, E.; Mohrmann, D.; Langhof, T.; Plappert, D.; Ledford, N.; Paul, H.; Hiermaier, S. A Simplified Design for a Split-Hopkinson Tension Bar with Long Pulse Duration. *Procedia Engineering* **2017**, *197*, 109–118. doi:10.1016/j.proeng.2017.08.087.
14. Koutny, D.; Skulina, D.; Pantělejev, L.; Paloušek, D.; Lenczowski, B.; Palm, F.; Nick, A. Processing of Al-Sc aluminum alloy using SLM technology. *Procedia CIRP* **2018**, *74*, 44–48. doi:10.1016/j.procir.2018.08.027.
15. Lee, W.S.; Chen, T.H. Dynamic Deformation Behaviour and Microstructural Evolution of High-Strength Weldable Aluminum Scandium (Al-Sc) Alloy. *Mater. Trans.* **2008**, *49*, 1284–1293. doi:10.2320/matertrans.MRA2008032.